

Geometrical models of interface evolution. II. Numerical simulation

David A. Kessler

Department of Physics, Rutgers University, Piscataway, New Jersey 08854

Joel Koplik and Herbert Levine

Schlumberger-Doll Research, P.O. Box 307, Ridgefield, Connecticut 06877

(Received 18 May 1984)

We continue our study of local interface models for dendritic growth by presenting detailed numerical simulations of the evolution of snowflake patterns. The local model we employ is quantitatively valid for early stages of the dendritic growth process and is qualitatively similar to the true diffusion-controlled dynamics as far as single-tip behavior is concerned. We show that a critical value of the crystal anisotropy must be exceeded before the system settles into stable tip and repeated side-branching behavior. Varying the anisotropy and measuring the dendrite velocity enables us to get a quantitative picture of the tip dynamics. In addition, we study global features of the evolving patterns, and find exponential growth for the curve complexity, $\xi \equiv [(\text{arclength})/(\text{area})^{1/2}]$. Our results are not consistent with a simple version of the marginal stability hypothesis of Langer and Müller-Krumbhaar.

I. INTRODUCTION

Much interest has been shown recently in the question of how nonlinear dynamical processes give rise to spatial patterns.^{1,2} We have argued that a class of simple systems, local interface models, can offer real insight in isolating those aspects of a growth process crucial to the resulting shape.^{3,4} This knowledge in turn will affect the methodology brought to bear on both the realistic partial differential equations which govern the physical system of interest and on experimental studies.

Many familiar examples of pattern formation can be found in crystal growth, when a solid seed is immersed in supercooled melt. The most striking phenomenon is the snowflakelike shape produced in growth via emission of dendritic branches, forming a complex yet highly ordered pattern.⁵ The equations governing the evolution of the pattern result from heat and/or concentration diffusion, coupled through nonlinear boundary conditions to the position and velocity of the solid-liquid interface. It is this problem which we choose to study using as our tool a local interface model.

In a previous paper⁶ (hereinafter referred to as I) we have introduced a simple class of dynamical systems which reproduce some of the features of pattern formation. These *local interface models* reduce the nonlocal dynamics of a two-phase system to a local evolution equation for the interface. In this paper we study the particular two-dimensional equation

$$\hat{n} \cdot \frac{d\vec{x}}{dt} = \left[\kappa + A\kappa^2 - B\kappa^3 + \frac{\partial^2 \kappa}{\partial s^2} \right] [1 + \epsilon \cos(m\theta)] \quad (1)$$

constructed so as to incorporate the physics of the solidification process. Equation (1) determines the time evolution of points \vec{x} on a (closed) interface parametrized by its

arclength s , curvature κ , and orientation angle θ (defined by $\cos\theta = \hat{n} \cdot \hat{y}$, where \hat{n} is the curve normal). A and B are physical parameters governing the growth. The term proportional to ϵ , not present in I, represents the effects of crystalline anisotropy. The motivation for this equation will be reviewed below. In I we showed that this equation with $\epsilon=0$ reproduces the Mullins-Sekerka instability⁷ and the Ivantsov needle-crystal solution⁸ of the heat-diffusion problem. Together with our initial numerical studies,³ we anticipated that the local model could reproduce many of the qualitative features of dendritic growth. Also, our model may be quantitatively valid during the early stages of pattern formation at large Peclet number, when the nonlocal effects have not yet become significant.

The principal result we wish to report in this current work, based upon extensive further numerical simulations of Eq. (1), is that the stable tip behavior and repeated side-branching characteristic of dendritic growth requires the presence of crystalline anisotropy, i.e., nonzero ϵ . This anisotropy has generally been assumed to be qualitatively unimportant, and so was ignored in most theoretical treatments of the solidification problem.⁹ Without sufficient anisotropy, dendritic tips split and stable growth ceases. Our numerical studies show that for ϵ greater than or equal to some critical value ϵ_c , depending on A , B , and m , our model does exhibit persistent dendritic tips and repeated side branching. This periodic side branching is associated with a damped oscillatory behavior of the tip velocity. The amount of damping decreases with decreasing ϵ , and for ϵ less than ϵ_c the oscillations grow with time. It is this instability which prevents dendritic growth without crystalline anisotropy.

Other features of our model can be investigated through numerical simulation. We have investigated the effect of the parameters A and B on the pattern morphology. The parameter A corresponds to the degree of undercooling,

and its variation can offer insight into the effect in the physical system of nonzero Peclet number. This is important because most simulations of the heat diffusion equation assume the limit of zero undercooling. Another issue is the sensitivity of our results to small changes in initial conditions. While the general structure of the pattern is relatively insensitive to such changes, the detailed shapes tend to diverge as soon as enough modes of the system are excited. This implies that the patterns formed by our system are not fixed points in any simple sense.

A qualitative deficiency of this local model is the absence of any interaction between different parts of the interface. Since the governing equation (1) is local, individual dendritic tips and side branches grow independently, and inevitably curve overlap occurs. The model lacks the realistic competition between tips, which results from the necessity of diffusing latent heat away during growth. Thus once overlap occurs, the model is only applicable to the growth near the tips, well away from the intersection region.

An important issue in the study of pattern formation is the complexity of the evolving structure. One can define a simple measure of the global complexity of the pattern ξ as the ratio of the interface's arclength to the square root of its enclosed area. We find that ξ grows exponentially with time, a reflection of the lack of tip competition. Computational difficulties result because as the interface grows increasingly complex, more and more interpolation points are required. This difficulty is endemic to any local model of growth, whether or not it contains additional field variables on the interface.⁴

The most important claim made throughout this work is that our model captures many of the essential features of dendritic growth. We expect that our major result, the necessity of a minimum anisotropy to support stable growth (by which we mean the existence of a dendritic tip which propagates at constant velocity), should be true in the real physical system. A recent numerical simulation¹⁰ of a realistic model of solidification, involving diffusing temperature fields, has verified the necessity of anisotropy. The many qualitative similarities between the results reported here and those of the realistic simulation support our assertion that our local model can serve as an excellent testing ground on which to extend our understanding of this problem.

The outline of this paper is as follows. In Sec. II we will review some of the ideas that lead to Eq. (1) and allow its reformulation as a differential equation for $\theta(s)$. We then describe our numerical algorithm. Section III focuses on the tip behavior and in particular on the oscillatory nature of the side-branch emission process. Section IV discusses global properties of the model, such as the behavior of the complexity. Section V deals with other issues such as the value of the critical anisotropy as a function of m as well as the effects of changing A or B . We show that the side-branch versus tip-splitting choice can be traced phenomenologically to the strength of the $2m$ th Fourier mode. Finally, Sec. VI summarizes the important lessons of this study, compares our work to other approaches in the literature, and gives suggestions for future work.

II. LOCAL GROWTH MODEL

In this section we review some results of our earlier paper on local evolution equations. We then discuss our numerical integration algorithm and explain how it was tested.

The key idea introduced in I is that many features of dendritic growth could be reproduced by assuming local curve evolution dynamics. The basic quantities entering into a local description are the arclength s , the curvature $\kappa(s)$, and $\theta(s)$ (the angle between the curve normal \hat{n} and a fixed direction, taken as the y axis). If we denote the right-hand side of (1) by $F(\theta)$, then we showed in I that this equation could be written in the equivalent form

$$\dot{\theta} = -\frac{\partial F}{\partial s}, \quad (2)$$

$$\dot{s} = \int_0^s \kappa(s') F(\theta(s')) ds', \quad (3)$$

where both θ and s may be taken to depend on some time-independent parametrization of the curve.

We find it convenient to introduce a relative arclength parametrization $\alpha \equiv s/s_T$, where s_T is the total arclength of the curve. Using

$$\frac{d}{dt} = \frac{\partial}{\partial t} \Big|_{\alpha} + \dot{\alpha} \frac{\partial}{\partial \alpha},$$

we can rewrite (3) as

$$\begin{aligned} \frac{\partial \theta(\alpha)}{\partial t} = & -\frac{1}{s_T} \frac{\partial F(\theta)}{\partial \alpha} \\ & -s_T \kappa(\alpha) \left[\int_0^\alpha \kappa F(\theta) d\alpha' - \alpha \int_0^1 \kappa F(\theta) d\alpha' \right], \end{aligned} \quad (4a)$$

$$\frac{\partial s_T}{\partial t} = s_T \int_0^1 d\alpha \kappa F(\theta), \quad (4b)$$

where $\kappa = (1/s_T)(\partial\theta/\partial\alpha)$.

Let us recall the physical significance of the components of (1). The fact that for small curvature the growth rate decreases as κ is due to the fact that in diffusive growth the radius $r(t) \sim \sqrt{t}$ at large times. The term in B represents a minimum bubble size; for large enough curvature, the solid recedes under the influence of its surface tension. This is also the origin of the term $d^2\kappa/ds^2$. One of the most important effects of surface tension is to act as a short-distance cutoff on the oscillation spectrum. It thereby establishes a physical length scale for the solidifying system, which we have taken to equal one. Our oscillation spectrum around a circle of radius r , for $\epsilon=0$, then takes the characteristic form

$$\dot{\delta}_n = \delta_n (n^2 - 1) \left[\frac{1}{r^2} \left[1 + \frac{2A}{r} - \frac{3B}{r^2} \right] - \frac{n^2}{r^4} \right]$$

for a perturbation of the form $\delta_n \cos(2\pi ns/s_T)$. Finally, the term in A corresponds to nonzero undercooling. Increasing A increases the growth rate and, as we shall see later, the sharpness of the pattern. We have allowed for the crystalline anisotropy of the solid with the factor $1 + \epsilon \cos(m\theta)$, where ϵ is the strength of the anisotropy

and m represents the crystal axes (i.e., $m=4$ for a square lattice and $m=6$ for hexagonal). This factor can originate in either the orientation dependence of the surface-tension coefficient or in asymmetric attachment kinetics.

We are mostly concerned with symmetric growth patterns rather than irregular or unstable patterns (such as Fig. 1 of Ref. 3). If we choose initial conditions with the same m -fold symmetry as the evolution equation (1), then (in the absence of computational error) the symmetry will be preserved in time. Similarly, the equation respects reflection symmetry about each m -fold symmetry axis if present in the initial conditions. We may then solve Eqs. (4) for the range $0 \leq \alpha \leq 1/2m$, and use the symmetry to extend the solution for the full range of α . The restriction to symmetric structures allows much more detail to emerge for a given amount of computer time.

Our numerical algorithm is quite straightforward. We assume an initial configuration in the form of a perturbed circle, $s_T = 2\pi r_0$, $\theta(\alpha) = 2\pi\alpha + (\delta/m)\sin(2\pi m\alpha)$. Equations (4) are discretized by letting $\alpha = j/2mn$, $j=0, 1, \dots, n$, giving rise to a set of coupled ordinary differential equations. We then use the predictor-corrector differential equation solver¹¹ LSODE to integrate this system. The input to this routine includes an evaluation of the Jacobian matrix $M_{\alpha\alpha'} \equiv \partial\theta(\alpha)/\partial\theta(\alpha')$, which we compute analytically using Eqs. (4). Finally, we reconstruct the physical curve by integrating $x(\alpha) = \int_0^\alpha \cos\theta(\alpha')d\alpha'$, $y(\alpha) = y_0 - \int_0^\alpha \sin\theta(\alpha')d\alpha'$. y_0 is chosen to ensure that the origin is the center of the pattern. The computation time scales as N^3 and a typical run of 300 points takes 8–10 h on the VAX 11/780 in double precision.

Several aspects of our algorithm should be noted. We have opted for the relative-arclength “gauge” which has the effect of rendering the evolution equations global in nature. In consequence the Jacobian matrix M is not banded or sparse and matrix inversion is slow. An alternate formulation, involving a time-independent parametrization would not have this problem. The cost, however, is that the arclength differences between the discretized points then vary in time so that derivatives become less accurate and dynamical reassignment of points is required. Our opinion is that while such reassignment may be useful for future computations, this method is more difficult to implement. Yet another possible method of solution involves direct discretization of (1) in (x, y) ; in fact we initially employed such a procedure but found the problems of interpolation and point reassignment too severe. Our method, based on (4), offers a simple scheme of easily testable accuracy.

We have performed several tests of the reliability of the program. First, we wrote an alternative program which integrated the equations using κ as the variable describing the curve. This program was then run and compared with the results of the θ program for the test case of a circle with $\delta=0.1$, $r_0=10$. The results agreed to within 10^{-4} for an integration time of 10 at $N=200$. Next, we compared our analytic evaluation of the Jacobian with a numerical Jacobian determination built into the LSODE package. This again agreed to the accuracy with which we were evaluating derivatives. For a last qualitative check, we ran the same initial curve, $r_0=8$, $\delta=3.6$ with the

same parameters $A=4$, $B=1.5$, $\epsilon=0.15$, $m=4$ at both 300 and 400 points. The results for $\kappa(s)$, shown in Figs. 1(a) and 1(b), dramatically show that all the observed detail of the side-branch train (which we will discuss later at great length) is independent of the spatial discretization.

A more detailed check of our algorithm can be made by using the mode analysis of the Appendix. There we truncate the evolution equations to a coupled set of ODE's for the first few Fourier modes of the curvature κ . If we keep only the first three modes,

$$\kappa(\alpha) = \kappa_0 + \kappa_1 \cos(2\pi m\alpha) + \kappa_2 \cos(4\pi m\alpha),$$

the time development of those three variables can be determined to arbitrarily high accuracy. We can then compare these values with a Fourier decomposition of the curvature as given by the results of our complete algorithm. Up to time $t=5$ for the test run the results agree to $O(10^{-5})$, which is the accuracy to which we expect the

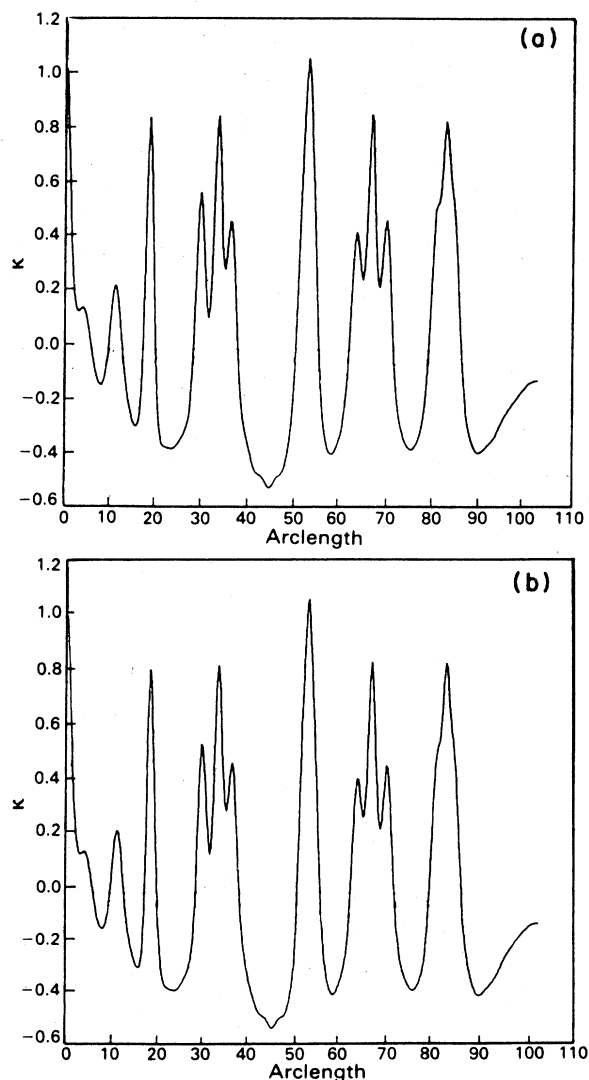


FIG. 1. Accuracy test: curvature vs arclength for a well-developed side-branch chain (a) using 300 interpolation points, (b) 400 points.

mode analysis to be a valid approximation. The combination of these checks assures us that the behavior of the interface is indeed being correctly determined by our numerical procedure.

III. DENDRITIC GROWTH

The first issue our model can address is the conditions necessary for dendritic patterns. We wish to know which parameters of the model, and by implication which physical mechanisms, control stable tip growth and repeated side branching. We find that a minimum value of the crystalline anisotropy is required.

In Fig. 2 we show the time evolution of a seed along

with a time sequence of curvature plots. This figure corresponds to $A=1$, $B=-\frac{1}{4}$, $N=200$, the initial conditions $r_0=10$ and $\delta=0.1$, and zero anisotropy. Notice that as time increases, the curvature peak at $s=0$ (corresponding to the primary tip) decreases and eventually splits into two peaks (only one shown). This peak then also splits, giving rise to a spatial pattern totally unlike a dendritic crystal. We have investigated a wide set of initial conditions and values of A and B , and it is always the case that $\epsilon=0$ gives rise to tips which split.

Next we study the effects of anisotropy. Figure 3 shows a time sequence with finite $\epsilon=0.085$, but still below ϵ_c , the critical anisotropy needed for tip stabilization. This simulation was done with $A=4$, $B=1.5$ and

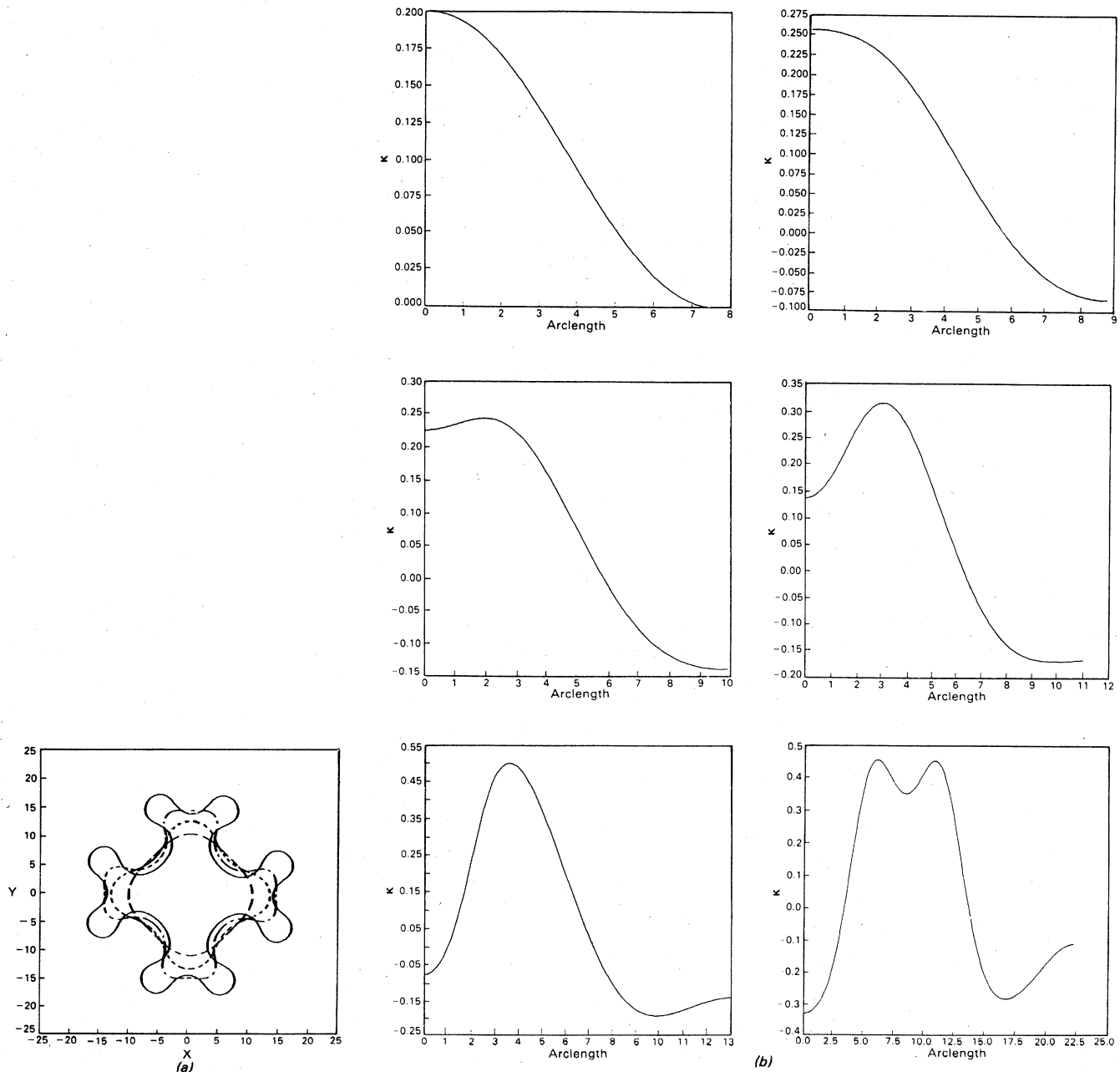


FIG. 2. Tip-splitting sequence ($A=1$, $B=0.25$, $\epsilon=0$): (a) evolving spatial pattern, (b) curvature plots at times $t=0, 6, 9, 12, 15, 21$.

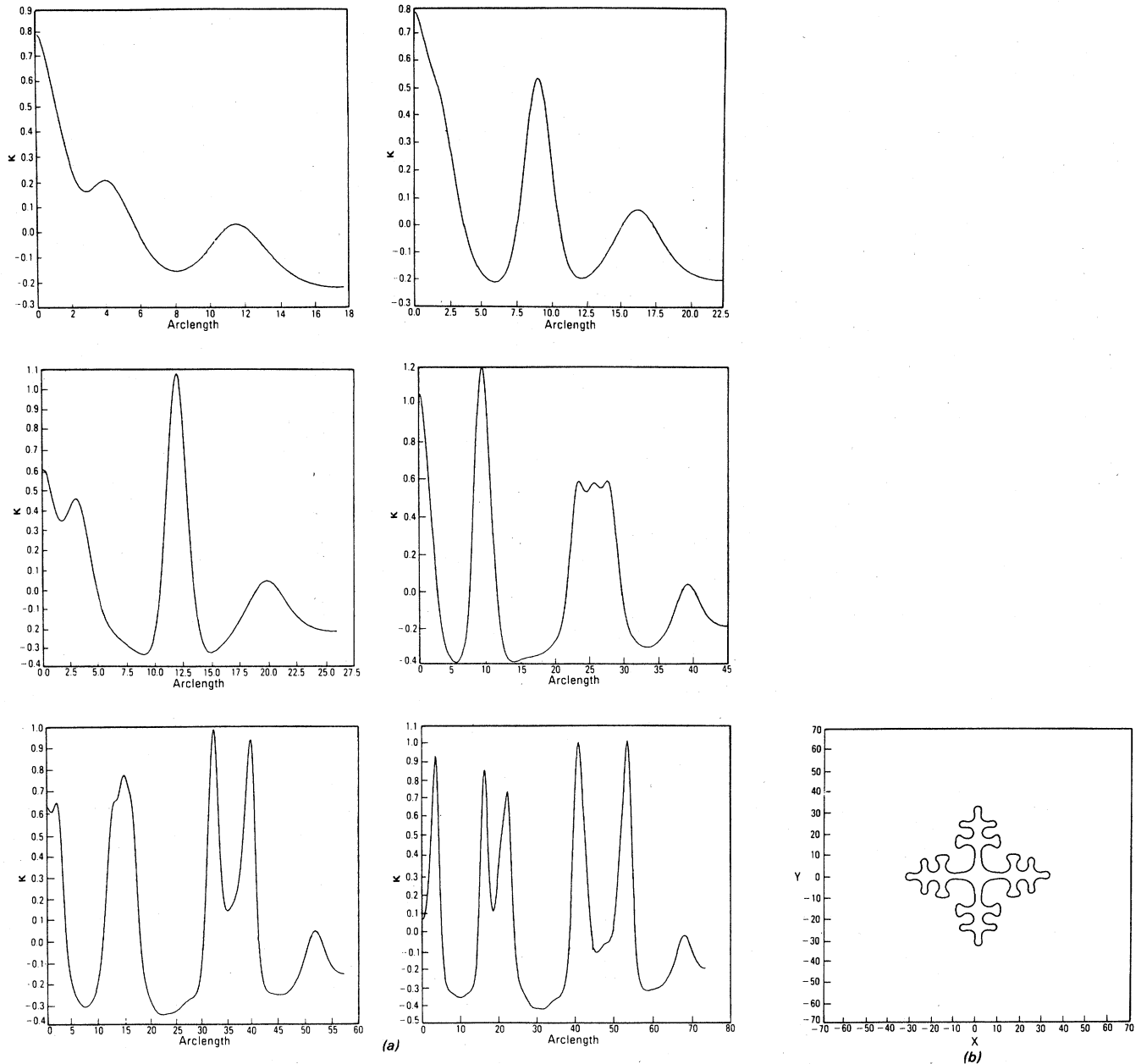


FIG. 3. Unstable side-branching sequence ($A=4$, $B=1.5$, $\epsilon=0.085$): (a) curvature plots at $t=0, 2.5, 5, 8, 11, 12$; (b) final state.

with initial conditions $r_0=8$, $\delta=3.6$. We have found by trial and error that this initial condition allows the system to settle into its side-branching behavior with a minimum of transient effects. Unless otherwise noted, all the remaining simulations will start from this initial configuration. We also choose $N=300$ as a compromise between accuracy and computer time.

Examining this example in detail, between times 2.5 and 5 we observe the beginning of a side branch. That is, the initial peak develops a shoulder which then becomes a new peak in the curvature plot. At time 11, we see that the first side branch has split and that the main peak (at $s=0$), while still present, is quite suppressed compared to earlier times. At the next time step the main peak disappears completely. This case is then a series of oscillations

which give rise to a few side branches before eventually decaying into tip-splitting behavior. We also show the spatial pattern at $t=11$, where one observes the broadening of the peaks (particularly the first side branch) which is the precursor of tip splitting. By $t=12$ the curve begins to overlap itself, which we discuss further in Sec. IV.

We next varied the anisotropy in small increments, keeping the other parameters fixed. As ϵ increases, the number of side branches the system emits before tip splitting occurs increases. For $\epsilon=0.05$, tip splitting takes place immediately. At $\epsilon=0.1$, four side branches are formed. At $\epsilon=0.125$, the system begins to go unstable only after approximately six completed cycles. Finally, at the critical value $\epsilon=0.15$, shown in Fig. 4, side-branching behavior stabilizes and the system may be capable of gen-

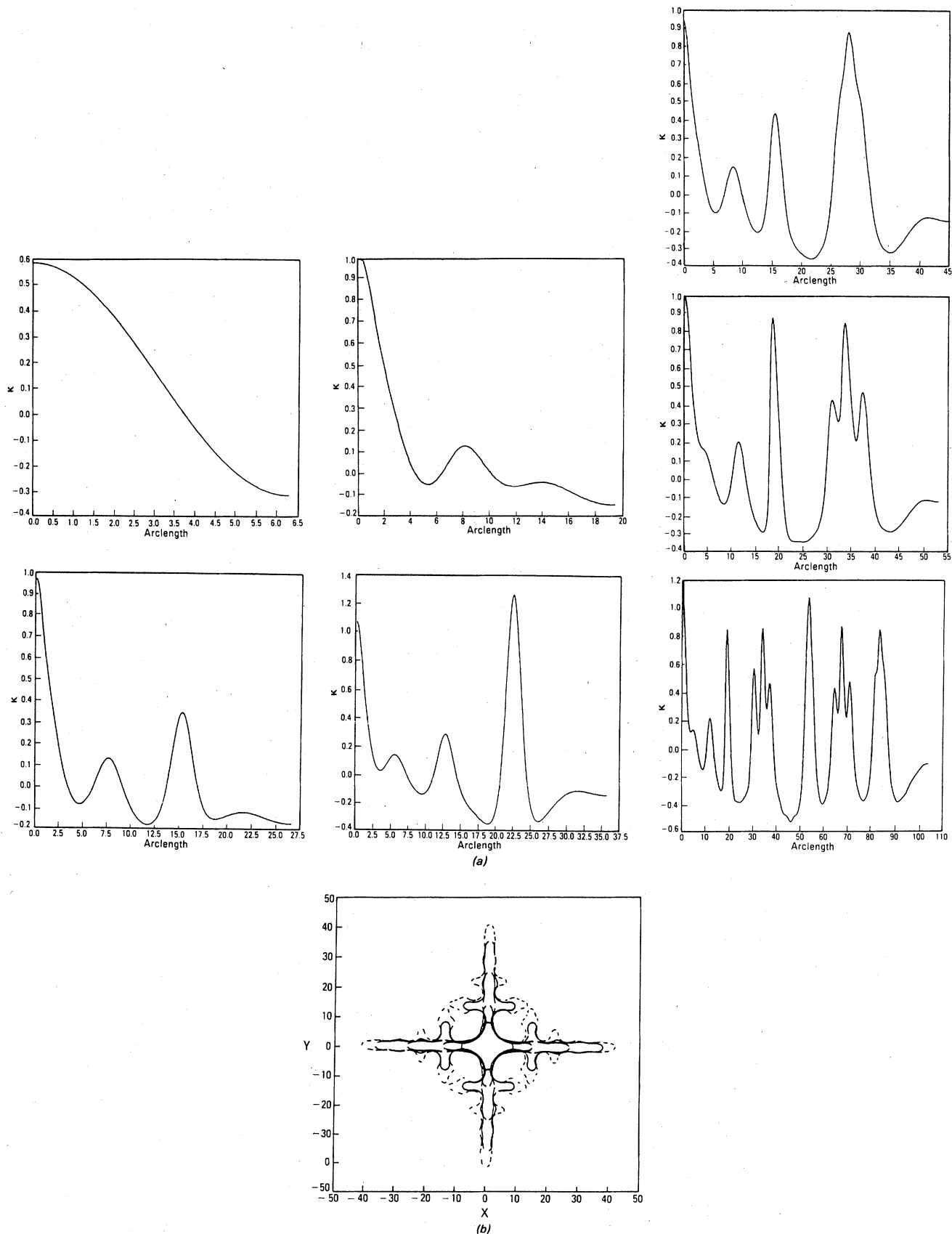


FIG. 4. Stable side-branching sequence ($A=4$, $B=1.5$, $\epsilon=0.15$): (a) curvature plots at $t=5, 8, 11, 13, 14, 15$; (b) evolving spatial pattern.

erating side branches indefinitely. Notice that the side branches themselves are stable and give rise to tertiary structure. For example, the first side branch develops a characteristic shoulder at $t=11$ and by $t=12$ has emitted two new curvature peaks. At $t=15$, the full structure corresponds to five secondary tips (initial side branches), the first of which has given rise to two tertiary tips, whereas the second has gone through one cycle (one tertiary tip) and, in fact, the beginnings of a fourth-level structure (at $s \sim 80$) is just beginning to emerge. Recall that this is just the case we have checked by also running at 400 points (see Fig. 1), so this detail is real and not a numerical error.

The shape of the dendrite tips in the late stages of growth in Fig. 4(b) resembles our model's analog of the Ivantsov needle crystal. In I we showed that in the absence of the $\partial^2 \kappa / \partial s^2$ term, Eq. (1) has uniformly translating solutions which away from the tip rapidly approach straight lines parallel to the growth direction. [For example, if $A=B=\epsilon=0$, the solution is $y=\rho \log \cos(x/\rho)$, with tip curvature $1/\rho$.] This general shape is seen to be a feature of the dendrite in Fig. 4(b) in the region between the main tip and the first side branch. In fact, ignoring the side branches, the baseline structure of the entire dendrite shares the feature of being almost exactly parallel to the propagation direction. It seems likely that the zero surface-tension steady-state shape is in some sense determining the true dendrite shape.

In Fig. 5 we plot the tip velocity as a function of time for a sequence of cases with increasing anisotropy. The oscillatory behavior exhibited is directly connected to the side-branch emission process. This can be verified by noting that each minimum in the tip velocity corresponds precisely to the point where the curvature shoulder develops into a new curvature maximum. When the anisotropy is subcritical, the oscillations in the tip velocity increase in amplitude and eventually cause a breakdown in the cyclic behavior. As ϵ is increased, the growth rate decreases, allowing for more branches before the collapse. Finally, at $\epsilon_c=0.15$, the growth ceases. Above this value the oscillations decrease in amplitude and the velocity settles down to a constant value $v \approx 2.6$.

The growing side branches also exhibit oscillatory behavior, roughly in phase with the principal dendrite. In Fig. 6 we show the main and first- and second-operation side-branch tip velocities as a function of time for the critical anisotropy case discussed above.

The one theoretical framework which proposes to explain the behavior of the tip is the marginal stability hypothesis of Langer and Müller-Krumbhaar.¹²⁻¹⁴ According to this suggestion the tip velocity is determined by the requirement that it is the smallest value such that perturbations about the tip are stable. We see, however, that this description is not in accord with the behavior of our model. In particular, for $\epsilon < \epsilon_c$, our system is manifestly unstable. The tip is not maintained in the time development of the system because it cannot "outrun" the side-branch modes propagating along the steady-state profile. In other words, the selected velocity is obviously less than what is needed to stabilize the tip, which thereafter splits apart.

One might suppose that the predictions of the marginal stability hypothesis are only valid in the stable tip regime, for large enough anisotropy. One could then compare the measured velocity with the velocity predicted by this approach. A simple modification of the calculation presented in I shows the predicted velocity to be $v \sim 1.6(1+\epsilon)$, independent of A and B .¹⁵ This does not agree with the above data, and, as we shall discuss in Sec. V, the velocity does depend strongly on A and B . Thus a better analysis of the tip behavior is necessary. The availability of our simple model will clearly aid in this process.

IV. GLOBAL PROPERTIES

In this section we investigate several global features of the patterns which emerge from our local geometrical equation. We examine some time-dependent measures of the evolving pattern related to arclength, enclosed area, and Fourier analysis of the shape.

A distinguishing feature of dendritic growth is the complexity of the boundary patterns which emerge. To quantify this property, it is useful to consider the enclosed area a , as well as the arclength of the curve. We then define the complexity ξ as the ratio s_T/\sqrt{a} . Increasing ξ corresponds to the development of more structure in the curve as it grows. In Fig. 7 we have plotted s_T , a , and ξ for a typical evolution. Aside from some oscillations, both s_T and a grow approximately exponentially in time and asymptotically ξ is nearly pure exponential. The same behavior is found for all cases we have studied.

There is a simple explanation for the exponential growth law. As we mentioned previously, any local model does not take into account competition between different parts of the interface. In consequence, each tip gives rise to a series of new tips at some fixed rate and each new tip in turn undergoes the same process, spawning a new set of branches. It is easy to see that the number of "distinct" pieces of the pattern is growing exponentially. Since there is no inhibition to the growth of any of these separate pieces, they cascade to give an exponentially increasing complexity. In a local model the interface will inevitably overlap itself after a sufficiently long time.

In any real physical system the secondary branches will be further away from the heat reservoir (or any other driving effect) than the primary tip. This means that the growth rate of the side branches should not be comparable to that of the primary branch—in the language of our model the effective parameters governing the side-branch evolution should be different than that giving the original dendritic growth. If one performs a simulation based on a nonlocal equation, one would expect to see only power-law time dependence for these objects.

A related phenomenon can be seen by considering a Fourier mode decomposition of $\kappa(\alpha)$. In Fig. 8 we present such an analysis for a case with $\epsilon=0.10 < \epsilon_c$. The abscissa is the m th Fourier component around the circle ($m=4$ in this case), with the distribution always normalized by $\kappa_0=1$. Note the steadily increasing number of modes which are "activated" in the course of time. This is unlike what occurs in more familiar pattern selection problems, such as Rayleigh-Bernard convection.¹⁶ In

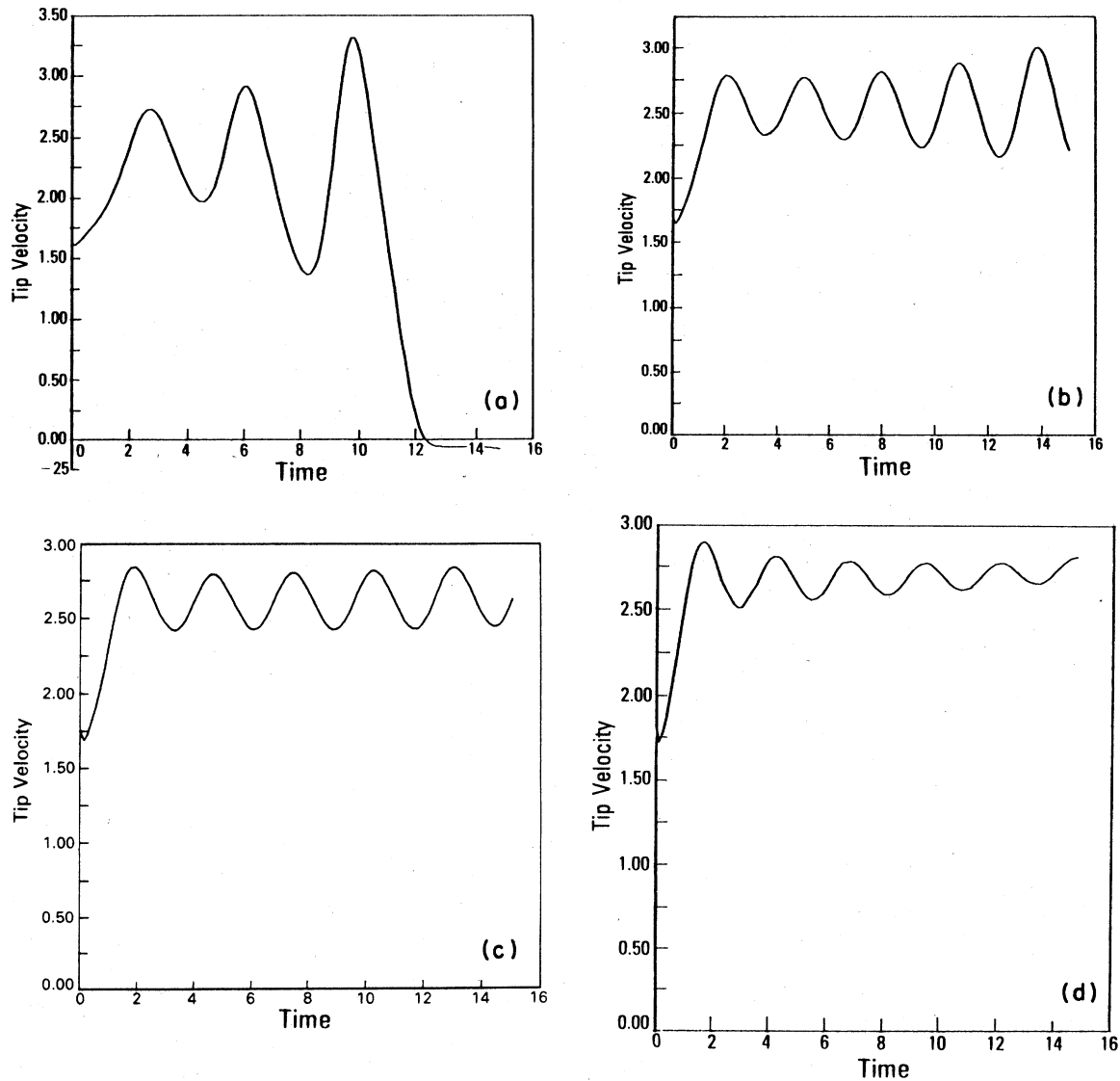


FIG. 5. Tip velocity vs time at various anisotropies ($A=4$, $B=1.5$): (a) $\epsilon=0.085$, (b) $\epsilon=0.125$, (c) $\epsilon=0.15$, (d) $\epsilon=0.2$.

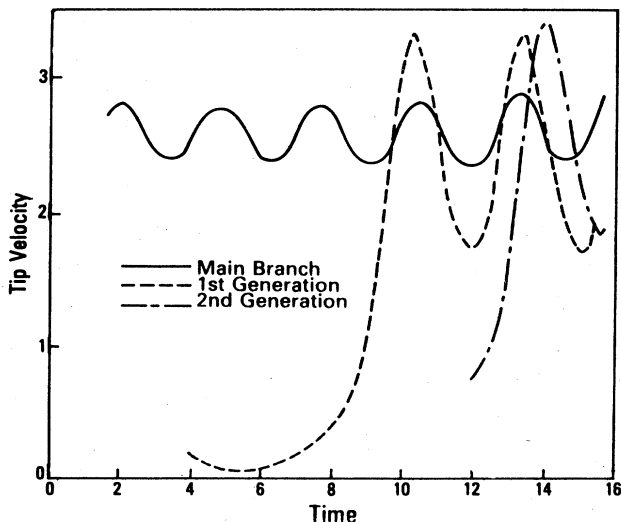


FIG. 6. Velocity of primary and secondary tips vs time ($A=4$, $B=1.5$, $\epsilon=0.15$).

those situations there is an external parameter (such as a temperature gradient) which when increased causes an instability to develop and thereby drives the system to a new stationary state. In dendritic growth the relevant size of the stabilizing (surface tension) and destabilizing (Mullins-Sekerka instability) tendencies changes with time, and as the system becomes larger, more modes become unstable. Inasmuch as our local equation models dendritic growth, it too has this property. We find that the number of modes of significant amplitude grows exponentially. Based on our experience with the complexity ratio, we would predict that this behavior is again an artifact of a local interface model.

The Fourier decomposition can also be used to predict whether for a given set of parameters (A, B, ϵ) the system tip splits or side branches. The key observation is that in Fig. 8(b) ($t=2.5$), the $n=2$ mode is suppressed relative to the $n=3$ mode. We examined this phenomenon further by using the initial conditions $r_0=10$, $\delta=1$ with $A=1$, $B=0$, where the evolution is initially less rapid. A com-

parison of a run with zero anisotropy and a run with 15% anisotropy is shown in Fig. 9; at least at this time, the relative amplitude of the $n=2$ mode is clearly different in the two cases. The importance of this result is the fact that one may be able to replace the full evolution equation by a mode truncation theme if one is only interested in estimating the critical anisotropy. This idea is developed in detail in the Appendix.

Lastly, one might ask if the patterns resulting from our model are "chaotic," in the sense of having strong sensitivity to initial conditions. A quantitative estimate can be given in terms of the separation between two patterns, defined as the area which is enclosed by one interface which is outside the other. Explicitly, if Ω_i is the interior region in pattern C_i , $i=1,2$, we define $\Delta \equiv \text{Area}(V)$, ($V \in \Omega_1$ and $V \notin \Omega_2$) or ($V \in \Omega_2$ and $V \notin \Omega_1$). We then slightly vary the initial conditions and plot Δ as a function of time. The results are shown in Figs. 10, where we have changed the initial deformation δ from 3.6 to 3.5 and 3.7 to generate second patterns. For t up to 6, Δ oscillates but does not grow and at later times Δ grows rapidly, approaching exponential separation. This again occurs for all cases we have examined.

V. VARIATION OF PARAMETERS

In the previous sections we have focused on general features of the patterns which emerge from our geometrical dynamics. The results presented so far are valid independent of the values of the parameters A and B , the crystalline symmetry m , and the initial conditions r_0, δ . We now discuss how variation of these quantities alters the pattern's behavior.

A qualitative indication of the possible change can be obtained by comparing Figs. 4 and 11. These two systems differ only in the value of B , respectively, 2 and 1.5. The effect of this change is that the primary tip, which is the highest curvature peak, is slowed relative to side-branch growth and the side branches are therefore more prominent. Because increasing B decreases the tip velocity, it is reasonable to expect that ϵ_c would be greater than the corresponding value at $B=1.5$. The velocity plot [Fig. 11(b)] clearly indicates that for this higher value of B , dendrite stability has not yet been achieved. The value of the tip velocity is decreased considerably as compared to Fig. 5(c), and the frequency of the oscillations has also decreased. If we decrease B to 1, the opposite behavior occurs. ϵ_c is now less than 0.15, the velocity increases, and the side-branch emission rate also increases.

We proceed analogously with the parameter A . If we increase A to 5 with other parameters fixed, the average tip velocity goes from 2.6 to 4.2. By the same reasoning as above, we now expect the value of ϵ we have used is greater than the critical value at this A , and this is found to be the case. If A is decreased to 1, one finds the reverse behavior. In general, the sensitivity to the value of A is much greater than the sensitivity to B .

It is premature to say much about which if any quantitative features of dendritic growth might be universal, in the sense of being independent of most of the physical parameters. While our simulations at fixed ϵ with varying

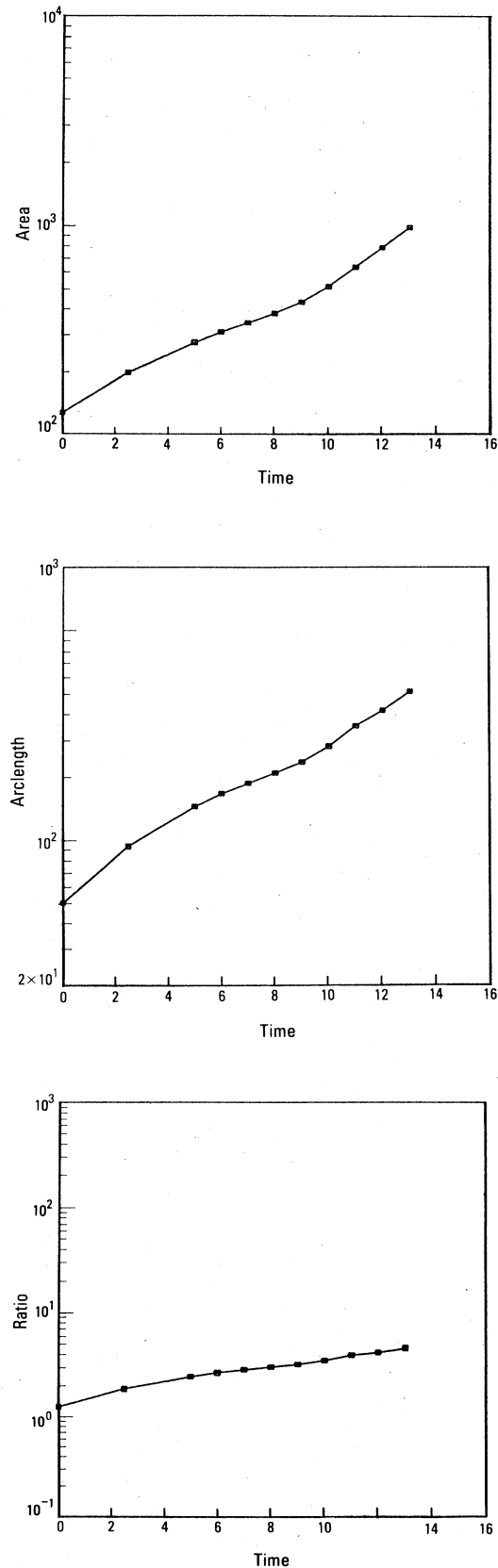


FIG. 7. Area, arclength, and complexity vs time ($A=4$, $B=1.5$, $\epsilon=0.15$).

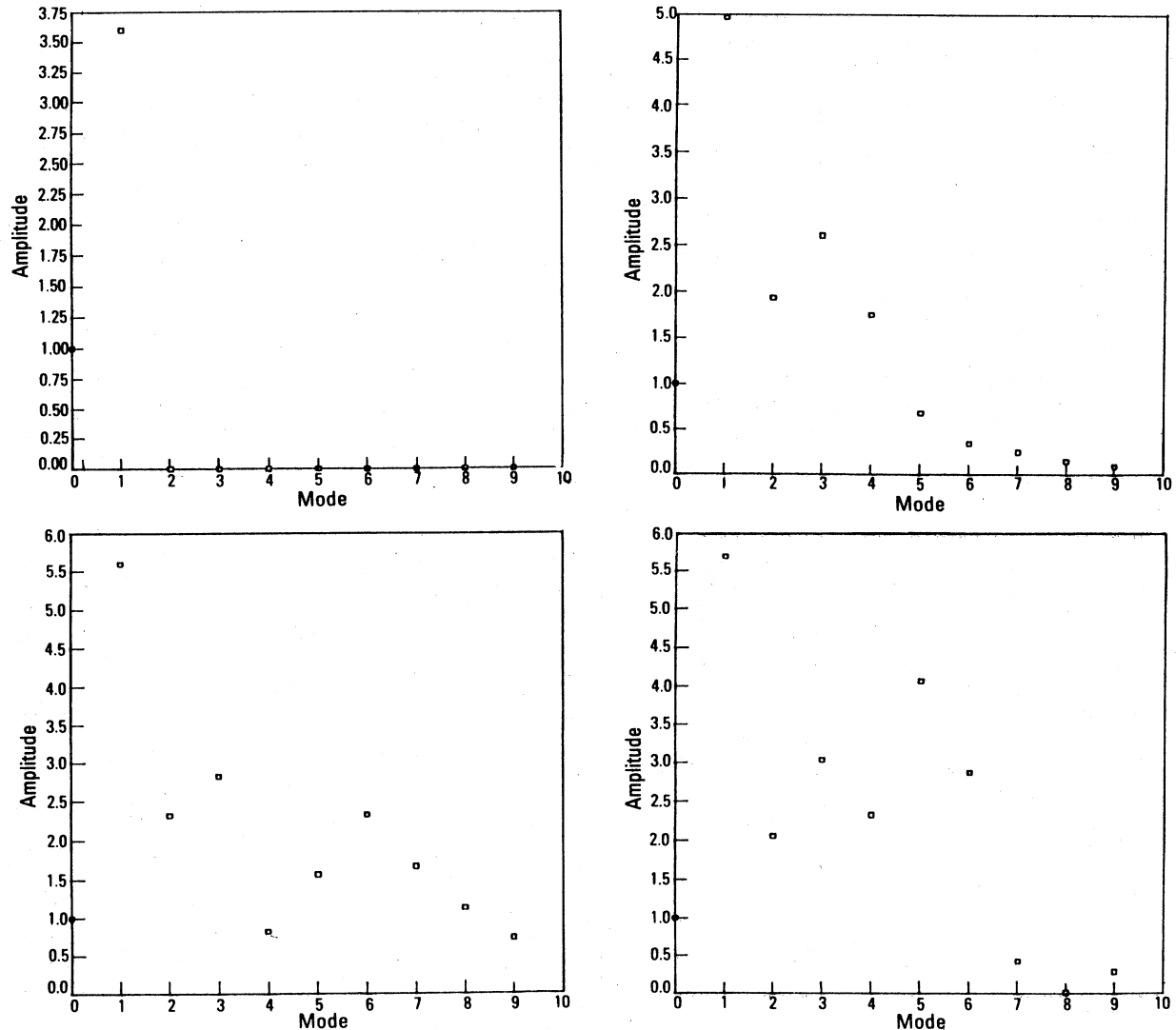


FIG. 8. Fourier coefficients at times $t=0, 2.5, 5, 6$ ($A=4$, $B=1.5$, $\epsilon=0.15$).

A and B give rise to different values for the tip-velocity and side-branch emission rate, there may be other quantities relevant to dendritic growth that are parameter independent. Alternatively, perhaps one must change the value of ϵ to be the same distance from the critical value before a meaningful comparison can be made. We hope to return to this question in the future.

A different issue is the effect of changing the initial conditions while keeping A and B fixed. We ran simulations with our standard set of parameters (those of Fig. 4) and varied the initial radius from 4 to 12. The tip velocity, oscillation frequency, and the critical value of ϵ were unchanged, but the amplitude of the oscillation varied with r_0 . Generally speaking, the closer the initial tip velocity was to the final average, the smaller the amplitude. Of course, the spatial pattern which emerges varies significantly from case to case, in line with the earlier discussion of the “chaotic” nature of the long time evolution of our equations. This point underlines again the range of usefulness of a local model—it will only model correctly local behavior such as tip oscillations, whereas the actual

pattern will depend in detail upon exactly what the starting configuration was.

Up to now we have considered the $m=4$ case, corresponding to cubic symmetry, and we now consider how the critical anisotropy changes with m . We find a dramatic variation, $\epsilon_c \sim 0.4-0.5$ for $m=5$ and $\epsilon_c \sim 0.7-0.8$ for $m=6$. This result may be an artifact of a local model. Linear stability analyses take the generic form, for a perturbation $\delta_n \sim \cos(n\theta)$,

$$\dot{\delta}_n \sim \delta_n m^2 n^2 (1 - \lambda_l m^2 n^2)$$

in the local model and

$$\dot{\delta}_n \sim \delta_n m |n| (1 - \lambda_f m^2 n^2)$$

in the diffusion equation.² For mode numbers n in the unstable region where $\delta_n > 0$, local models predict more rapid instability as a function of m which may require increased ϵ for stabilization of the tip. The numerical value of the critical anisotropy is surely model dependent.

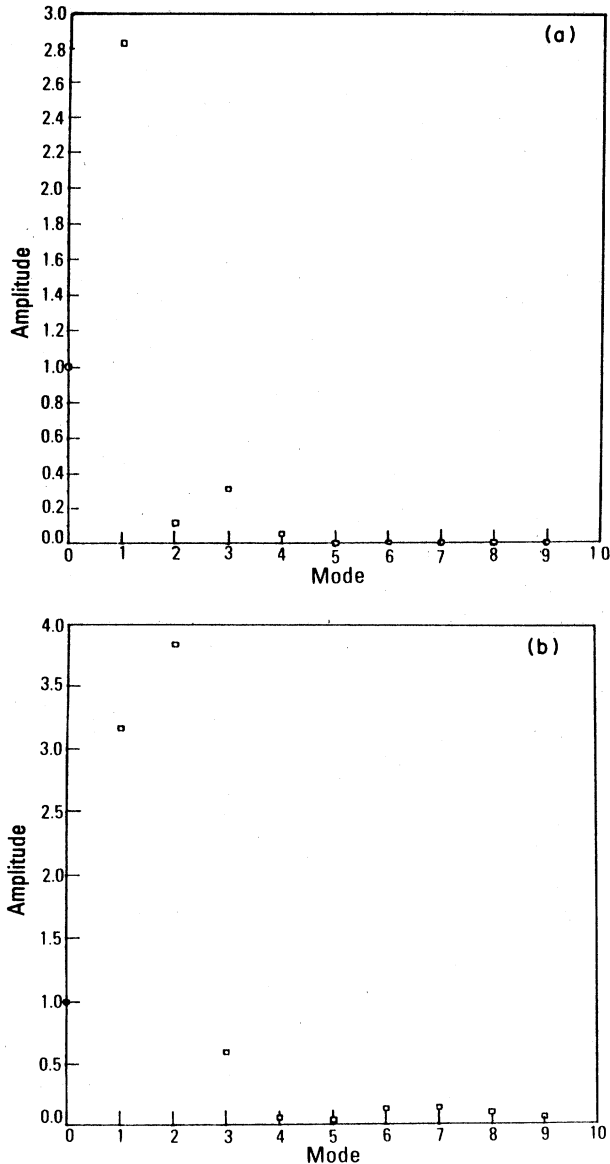


FIG. 9. Comparison of Fourier coefficients at $t=9$ for (a) tip splitting ($A=1, B=0, \epsilon=0$), (b) side branching ($A=1, B=0, \epsilon=0.15$).

VI. DISCUSSION

We have provided evidence based on numerical simulations that our local growth model gives rise to interesting phenomena in the course of its time evolution. Specifically, we have introduced the critical anisotropy as well as the pattern complexity as a way of characterizing some of these numerical results. We hope to apply these concepts to more realistic diffusion-controlled processes and sort out which aspects of dendritic growth are insensitive to the specific evolution equation used and are therefore universal features of this type of pattern formation.

Much of the preceding discussion has dealt with the qualitative and phenomenological behavior of the dendritic tip. The next step is to formulate a theory which predicts such quantities as the tip velocity and side-branch spacing. For the first time, any such theory can be com-

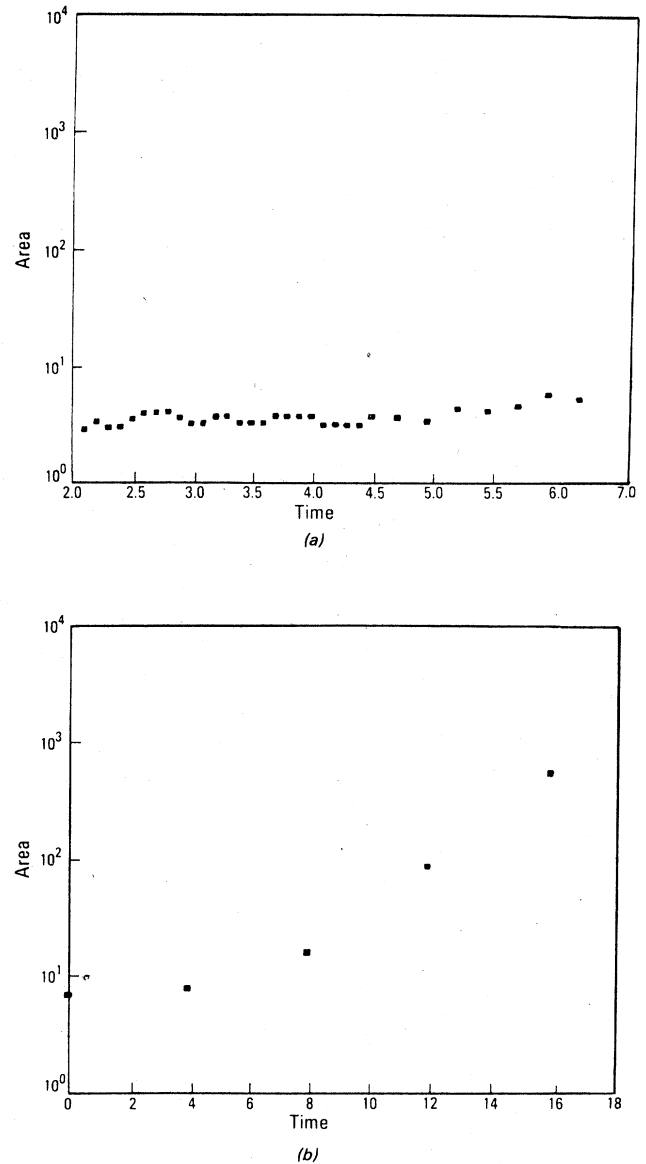


FIG. 10. Area comparison (see text for definition): (a) early times, (b) late times.

pared directly to precise computer simulations. It may or may not be appropriate to incorporate some form of the marginal stability hypothesis, which to date has only been established for some one-dimensional partial differential equations.¹³ As we have pointed out, a comparison of our results with the simplest version of this hypothesis show it to be incorrect.

The pattern in Fig. 2 resembles certain biological cells;¹⁷ indeed, one might model the growth of a cell in a nutrient bath by Eq. (1) with $\epsilon=0$. Circular growth would have the concentration analog of the thermal Mullins-Sekerka instability, an outward bump on the interface (cell wall), seeing a higher nutrient concentration and growing faster, counterbalanced by surface tension tending to keep the wall compact. This is an interesting area for future study.

Let us contrast our model and its numerical implemen-

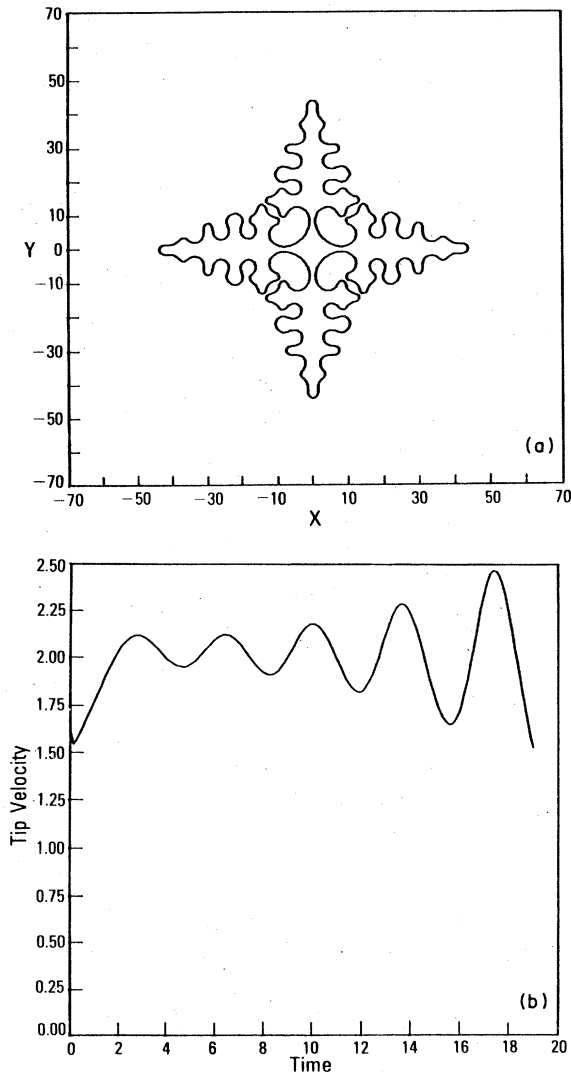


FIG. 11. Effect of charging B ($A=4$, $B=2$, $\epsilon=0.15$): (a) final spatial pattern, (b) side-branch train, at $t=18$.

tation with several other approaches to growth processes. First, there are models in which an object grows by the random aggregation of particles (or clusters) undergoing diffusive motion. The best known of these is diffusion-limited aggregation (DLA), introduced by Witten and Sander.¹⁸ This system gives rise to fractal, disorderly patterns by screening the inner parts of the structure by the furthest dendritic arms. This model also has the attractive feature of being easy to simulate. From our point of view, though, this model cannot hope to explain the orderliness and symmetry which grace dendritic patterns in many solidification experiments. Our model builds in the local mechanisms that allow for such order, albeit at the cost of neglecting the global competition present in DLA.

Another possibility is to use cellular automata¹⁹ to model crystal growth. The advantages of this method is again one of computational facility. The disadvantages are, we feel, quite serious. One loses the ability to investigate questions such as the effect of crystal anisotropy, inasmuch as the entire growth procedure is always aniso-

tropic. Furthermore, since cellular models are intrinsically discrete, it is difficult to obtain a useful continuum description (this is true of DLA as well). Two-dimensional dendritic growth is a system that *can* be studied by more standard computational techniques, and we therefore believe our approach to be more useful.

Finally, one can augment the simple geometrical dynamics of Eq. (1) by additional fields which incorporate other physical mechanisms. An example is the boundary-layer model recently introduced by Ben-Jacob *et al.*⁴ This model is still a local model in the sense of not including the competitive effects that are present in DLA or in the true heat-diffusion equations. It can therefore never be completely realistic inasmuch as this effect is obviously important. However, it is much more cumbersome to implement numerically, simply because of the extra variables. We believe that since that model is only marginally closer to the true physics than the simple evolution of Eq. (1), it does not justify the extra computational complexity.

As noted in the Introduction, reliable numerical computations have recently been performed for the first time on a realistic diffusion model of dendritic growth.¹⁰ We are thus able to compare the behavior of our simple model directly to that of a more physical (and computationally much more expensive) simulation. The crucial point is that the results of Ref. 10 show that the idea of a critical anisotropy is not just a property of local models, but that it carries over to the full diffusion dynamics. We can therefore confidently predict that any system undergoing domain growth will eventually give rise to disorderly, tip-splitting behavior in the absence of any symmetry breaking (such as sufficiently large crystalline anisotropy) in the evolution equations.

Two other points of comparison should be noted. The profiles seen in the diffusion-equation simulations appear qualitatively different from those seen here. This difference is presumably attributable to the differing steady-state dendrite shapes present in the two systems. In particular, the diffusion equation gives rise to parabolic dendrite solutions, a fact clearly reflected in Fig. 2 of Ref. 10. Finally, the complexity measure ξ obeys the power law $\xi \sim t^\gamma$ as a result of the nonlocal competition between tips. This is consistent with the discussion of Sec. IV.

In conclusion, we have demonstrated that our model is a valuable tool for elucidating the nature of pattern-formation mechanisms. Our model represents an effective compromise between simplicity and physical principles, allowing us to identify the crucial features of solidification. The obvious next step is to use the results here to develop a quantitative understanding of dendritic tip behavior.

APPENDIX

In this appendix we derive a mode truncation scheme for our local equation and show how this might be used to predict the order of magnitude of the critical anisotropy. There are many complicated global evolution laws which are not currently amenable to computer simulation which might be treated by such a mode truncation. If one could

develop an approximate signal for tip splitting from the very early stage evolution when the mode approach is reliable, behavior of these more complicated systems could be estimated.

We approximate the curvature by the four-mode truncation

$$\kappa = \sum_{n=0}^3 k_n \cos(2\pi n \alpha),$$

along with a similar decomposition for $\theta(\alpha)$. Substituting into the evolution equation (4a) and (4b) identifying the coefficients of different Fourier components, we can derive evolution equations for the four unknown coefficients k_0, k_1, k_2, k_3 .

At $\epsilon=0$ we can perform the computation analytically to find (with $s_T=2\pi/k_0$)

$$\dot{k}_0 = - \left[k_0^2 + \frac{k_1^2}{2} \right] + A(k_0^3 + \frac{3}{2}k_0k_1^2 + \frac{3}{4}k_1^2k_2) + B(k_0^4 + 3k_0^2k_1^2 + 3k_0k_1^2k_2 + \frac{3}{8}k_1^4 + \frac{1}{2}k_1^3k_3) - \left[\frac{2\pi m}{s_T} \right]^2 \frac{k_1^2}{2},$$

$$\begin{aligned} \dot{k}_1 = & -(3k_0^2k_1 + \frac{5}{8}k_1^3 + \frac{1}{2}k_0k_1k_2 + \frac{1}{8}k_1^2k_3) - A(4k_0^3k_1 + \frac{21}{8}k_0k_1^3 + \frac{9}{4}k_0^2k_1k_2 + \frac{9}{8}k_0k_1^2k_3 + \frac{19}{24}k_1^3k_2) \\ & - B(5k_0^4k_1 + 5k_0^3k_1k_2 + \frac{15}{4}k_0^2k_1^2k_3 + \frac{27}{4}k_0^2k_1^3 + \frac{31}{6}k_0k_1^3k_2 + \frac{1}{2}k_1^5 + \frac{49}{64}k_1^4k_3) \\ & + \left[\frac{2\pi m}{s_T} \right]^2 \left[k_1 + 2A(k_0k_1 + \frac{1}{2}k_1k_2) + 3B(k_0^2k_1 + k_0k_1k_2 + \frac{1}{4}k_1^3 + \frac{1}{4}k_1^2k_3) \right. \\ & \left. + (k_0^2k_1 + 3k_0k_1k_2 + \frac{5}{8}k_1^3 + \frac{9}{8}k_1^2k_3) \right] - \left[\frac{2\pi m}{s_T} \right]^2 k_1, \end{aligned}$$

$$\begin{aligned} \dot{k}_2 = & -(3k_0^2k_2 + \frac{5}{2}k_0k_1^2 + \frac{1}{3}k_0k_1k_3 + \frac{11}{6}k_1^2k_2) - A(4k_0^3k_2 + \frac{9}{2}k_0^2k_1^2 + k_0^2k_1k_3 + 7k_0k_1^2k_2 + \frac{5}{6}k_1^4 + \frac{1}{2}k_1^3k_3) \\ & - B(5k_0^4k_2 + 7k_0^3k_1k_2 + \frac{10}{3}k_0^3k_1k_3 + 17k_0^2k_1^2k_2 + \frac{23}{6}k_0k_1^4 + \frac{7}{2}k_0k_1^3k_3 + \frac{93}{32}k_1^4k_2) \\ & + \left[\frac{2\pi m}{s_T} \right]^2 \left[4k_2 + 2A(4k_0k_2 + k_1^2 + 2k_1k_3) + 3B(4k_0^2k_2 + 2k_0k_1^2 + 4k_0k_1k_3 + 2k_1^2k_2) \right. \\ & \left. + (4k_0^2k_2 + \frac{3}{2}k_0k_1^2 + 7k_0k_1k_3 + \frac{23}{6}k_1^2k_2) \right] - \left[\frac{2\pi m}{s_T} \right]^2 16k_2, \end{aligned}$$

$$\begin{aligned} \dot{k}_3 = & -(3k_0^2k_3 + \frac{11}{2}k_0k_1k_2 + \frac{3}{8}k_1^3 + \frac{13}{8}k_1^2k_3) - A(4k_0^3k_3 + \frac{39}{4}k_0^2k_1k_2 + \frac{11}{8}k_0k_1^3 + \frac{51}{8}k_0k_1^2k_3 + \frac{81}{32}k_1^3k_2) \\ & - B(5k_0^4k_3 + 15k_0^3k_1k_2 + \frac{13}{4}k_0^2k_1^3 + \frac{63}{4}k_0^2k_1^2k_3 + \frac{93}{8}k_0k_1^3k_2 + \frac{27}{64}k_1^5 + \frac{33}{16}k_1^4k_3) \\ & + \left[\frac{2\pi m}{s_T} \right]^2 \left[9k_3 + 2A(9k_0k_3 + \frac{9}{2}k_1k_2) + 3B(9k_0^2k_3 + 9k_0k_1k_2 + \frac{3}{4}k_1^3 + \frac{9}{2}k_1^2k_3) \right. \\ & \left. + (9k_0^2k_3 + 7k_0k_1k_2 + \frac{3}{8}k_1^3 + \frac{49}{8}k_1^2k_3) \right] - \left[\frac{2\pi m}{s_T} \right]^2 81k_3. \end{aligned}$$

At nonzero anisotropy each of the above equations is supplemented by a term on the right-hand side proportional to ϵ . These terms were evaluated by MACSYMA with a given set of value for the k_n, \dots . Although we cannot present an analytic formula, we can still integrate the above equation by calling this determination as a subroutine during the numerical implementation of the time evolution of this mode truncated system.

We noted in Sec. IV that the relative suppression of the $n=2$ mode was indicative of tip splitting, at least for $m=4$. In the following tables we demonstrate that our mode truncation scheme is capable of yielding this type of information for the case shown in Fig. 10. For $\epsilon=0$ [Eq. (1)],

t	k_0	k_1	k_2	k_3
0	0.1	0.1	0	0
3	0.0945	0.141	0.001	-0.001
6	0.0878	0.186	0.002	-0.007
9	0.079	0.225	-0.009	-0.02

and for $\epsilon=0$ (mode scheme)

t	k_0	k_1	k_2	k_3
0	0.1	0.1	0	0
3	0.095	0.142	0.001	-0.002
6	0.088	0.187	0.002	-0.005
9	0.079	0.23	-0.006	-0.015

Now we increase the value of ϵ to 0.15 and find, from Eq. (1),

t	k_0	k_1	k_2	k_3
0	0.1	0.1	0	0
3	0.094	0.146	0.05	0.03
6	0.087	0.192	0.159	0.10
9	0.068	0.221	0.26	0.11

and for $\epsilon=0.15$ (mode scheme)

t	k_0	k_1	k_2	k_3
0	0.1	0.1	0	0
3	0.094	0.147	0.05	0.03
6	0.087	0.196	0.17	0.09
9	0.076	0.231	0.36	0.15

Although the accuracy is somewhat degraded, the difference between these tables and the zero anisotropy case is clear. If this method survives further investigation, it will be possible to easily estimate the anisotropy necessary to yield stable dendrites in our local model, and perhaps this approach could predict critical anisotropies for physically relevant metallurgical systems.

¹Proceedings of the Los Alamos Conference on Fronts, Interfaces and Patterns [Physica D 12, 1 (1984)].

²J. S. Langer, Rev. Mod. Phys. 52, 1 (1980).

³R. C. Brower, D. A. Kessler, J. Koplik, and H. Levine, Phys. Rev. Lett. 51, 1111 (1983).

⁴E. Ben-Jacob, N. Goldenfeld, J. S. Langer, and G. Schön, Phys. Rev. Lett. 51, 1930 (1983); Phys. Rev. A 29, 330 (1984).

⁵U. Nakaya, *Snow Crystals* (Harvard University, Cambridge, Mass., 1954).

⁶R. C. Brower, D. A. Kessler, J. Koplik, and H. Levine, Phys. Rev. A 29, 1335 (1984).

⁷W. W. Mullins and R. W. Sekerka, J. Appl. Phys. 34, 323 (1963); 35, 444 (1964).

⁸G. P. Ivantsov, Dok. Akad. Nauk SSSR 58, 567 (1947).

⁹See, however, J. W. Cahn, in *Crystal Growth*, edited by H. S. Peysner (Pergamon, New York, 1967); S.-K. Chan, H.-H. Reimer, and M. Kahlweit, J. Cryst. Growth 32, 303 (1976).

¹⁰D. A. Kessler, J. Koplik, and H. Levine Phys. Rev. A (in press).

¹¹A. C. Hindmarsh, ACM-Signum Newsletter 15, 10 (1980).

¹²J. S. Langer and H. Müller-Krumbhaar, Acta Metall. 26, 1681 (1978); 26, 1689 (1978); 26, 1697 (1978); Phys. Rev. A 27, 499 (1983). For a discussion of experimental tests of this idea, see S.-C. Huang and M. E. Glicksman, Acta Metall. 29, 701 (1981); 29, 717 (1981).

¹³D. G. Aronson and H. F. Weinberger, Adv. Math. 30, 33

(1978); G. Dee and J. S. Langer, Phys. Rev. Lett. 50, 383 (1983).

¹⁴E. Ben-Jacob, H. Brand, G. Dee, L. Kramer, and J. S. Langer (unpublished).

¹⁵The marginal stability analysis presented in I and quoted here makes use of the continuous spectrum around the asymptotic dendritic shape. In general, one might find additional unstable modes corresponding to bound states in the region closer to the tip (referred to as Case II in Ref. 14). These modes would then require a higher velocity to become stable and would allow for the possibility of a dependence on A and B . In general, the calculation cited offers only a lower bound on the velocity. Inasmuch as this type of complication does not occur in the oscillation spectrum of the full heat-diffusion equation, we consider it unlikely that our model exhibits important bound-state modes.

¹⁶*Hydrodynamic Stability and the Transition to Turbulence*, edited by H. L. Swinney and J. P. Gollub (Springer, Berlin, 1981).

¹⁷O. Kiermayer, *Cell Biology Monographs* (Springer, Berlin, 1981), Vol. 8, p. 147.

¹⁸T. A. Witten, Jr. and L. M. Sander, Phys. Rev. Lett. 47, 1400 (1981); Phys. Rev. B 27, 5686 (1983).

¹⁹S. Wolfram, Rev. Mod. Phys. 55, 601 (1983); N. Packard and S. Wolfram (unpublished).